The Central Strain Analytical Modeling and Analysis for the Plate Rolling Process

Lian-Yun Jiang
Taiyuan University of Science and Technology
Yaoyu Wei (tyustsantu@163.com)
Taiyuan University of Science and Technology
Heng Li
Taiyuan University of Science and Technology
Li-feng Ma
Taiyuan University of Science and Technology

Research Article

Keywords: Stream function, Boundary conditions, Velocity field, Equivalent strain model, Plate rolling

Posted Date: July 30th, 2021

DOI: https://doi.org/10.21203/rs.3.rs-755524/v1

Version of Record: A version of this preprint was published at The International Journal of Advanced Manufacturing Technology on October 6th, 2021. See the published version at https://doi.org/10.1007/s00170-021-08148-2.

The Central Strain Analytical Modeling and Analysis for the Plate Rolling Process

Lian-Yun Jiang[1], Yao-Yu Wei[1,*], Heng Li[1], and Li-feng Ma[1]

**Correspondence author. E-mail: tyustsantu@163.com*

[1] School of Mechanical Engineering, Taiyuan University of Science and Technology, Taiyuan 030024, PR China

Abstract: The strain after rolling plays an important role in the prediction of the microstructure and properties and plate deformation permeability. So it is necessary to establish a more accurate theoretical strain model for the rolling process. This paper studies the modeling method of the equivalent strain based on the upper bound principle and stream function method. The rolling deformation region is divided into three zones (inlet rigid zone, plastic zone, and outlet rigid zone) according to the kinematics. The boundary conditions of adjacent deformation zones are modified according to the characteristics of each deformation zone. A near-real kinematics admissible velocity field is established by the stream function method on this basis. The geometric boundary conditions of the deformation region are obtained. The deformation power, friction power and velocity discontinuous power are calculated according to the redefined geometric boundary conditions. On this basis, the generalized shear strain rate intensity is calculated according to the minimum energy principle. Finally, the equivalent strain model after rolling is obtained by integrating the generalized shear strain rate in time. The plate rolling experiments of AA1060 and the numerical simulations are carried out with different rolling reductions to verify the analytic model precision of the equivalent strain. The results show that the minimum and maximum relative equivalent strain deviation between the analytic model and the experiment is 0.52% and 9.96%, respectively. The numerical calculation and experimental results show that the model can accurately calculate the strain along the plate thickness. This model can provide an important reference for the rolling process setup and the microstructure and properties prediction.

Keywords: Stream function; Boundary conditions; Velocity field; Equivalent strain model; Plate rolling.

Nomenclature

H	Initial plate thickness.
h	Plate thickness after rolling.
Δh	Reduction.
L	Length of the deformation region.
Γ_1, Γ_2	Velocity discontinuities.
R	Radius of the top and bottom work rolls.
Φ	Flow in the unit section.
$y_1(x)$	Geometric equation of rolling contact arc.
$y_2(x)$	Geometric equation of Γ_1.
$y_3(x)$	Geometric equation of Γ_2.
σ_s	Yield strength.
k	Shear yield strength.
m	Friction coefficient.
x, y	Cartesian coordinates.
a, b	Correction factor of the streamline.
α	The angle between the tangent of velocity discontinuity (Γ_1) and horizontal direction.
β	The angle between the tangent of velocity discontinuity (Γ_2) and horizontal direction.
v_0	Inlet velocity.
v_1	Outlet velocity.
v_x	Horizontal velocity component.
v_y	Vertical velocity component.
$\dot{\varepsilon}_x$	Strain rate along the x direction.
$\dot{\varepsilon}_y$	Strain rate along the y direction.
W	Total power.
W_V	Power consumed in deformation region.
W_f	Power with the friction by the work roll.
$W_{\Gamma 1}$	Power consumed in inlet velocity discontinuities.
$W_{\Gamma 2}$	Power consumed in outlet velocity discontinuities.
Λ	Cumulative shear strain strength.

$\dot{\Gamma}$ Generalized shear strain rate intensity.

1. Introduction

The metal plate which is the basic industrial material has been widely used in plenty fields, such as aerospace, bridge, shipping and so on [1-2]. A majority metal plate is produced by the rolling method. There is not a reliable method to measure the equivalent strain during rolling online, so the strain is unknown during the rolling production process [3]. So the soft measuring method can be introduced to predict the strain along the thickness, which is the key to predict the microstructure and properties and the reference for the process parameters setup. The soft measuring method needs a reliable analytic strain model, so the key problem about how to establish a reliable analytic strain model will be solved in this paper.

As the most convenient method, the numerical method has been widely used in the analysis of the metal rolling process. Hacquin et al. [4] simulated thermo-elastic rolling process with a steady-state thermo-elastoviscoplastic finite element model, and obtained the stress-strain variation law for the strip rolling process. Su et al. [5] developed a Fortran program that combined the three-dimensional rigid-plastic finite element method and slab method. This program can quickly calculate the strain during the rolling process. Denis pustovoytov et al. [6] used rigid plastic finite element method to simulate the asymmetric rolling process of magnesium-aluminum alloy, and the relationship between strain gradient and speed ratio was obtained. Bian et al. [7] simulated the gradient temperature rolling (GTR) and obtained the strain affecting rule. Matthias Schmidtchen et al. [8] established a fast finite element model of asymmetric compound rolling based on the improved slab theory and the actual situation of non-uniform plane strain deformation. These results can provide a good basis for the analysis of the rolling process, especially for the stain calculation.

Many scholars have also established some analytic models based on slab method, upper bound method and energy method, such as the strain, rolling force and so on, to improve the calculation speed of rolling process parameters. Jiang et al. [9] modified Von-Mises yield criterion and calculated mechanical parameters of the snake rolling process by the slab method. The accuracy of the model is in good agreement with the numerical results. Zhao et al. [10] established the power consumption model by the upper bound method and the linearized yield

criterion, the rolling force was calculated with good precision compared to the data measured in the factory. Zhang et al. [11] obtained the functional relationship between the stress state coefficient and the crack defect by using the upper bound theorem. The shape dependent criterion of the closed rectangular defect in the hot rolling process was established on this basis. The success of these calculation methods provides an effective and feasible idea for the rolling strain calculation.

The stream function method can be used to analyze the kinematic process of metal plastic forming as an upper bound method. S.I. Oh and Kobayashi [12] taken the extremum principle to analyze the three-dimensional rolling process for the ideal rigid plastic materials. Bayoumi [13] established the metal flow model of the bar during the rolling process by the flowline field method. The velocity strain rate and stress components were solved, and the process parameters affecting the law were analyzed. Wang et al. [14] built a model to predict the free boundary profile for the metal forming based on the stream function method. Maity et al. [15] made an upper bound analysis for the billet extrusion. The kinematically admissible velocity field was calculated by using the dual stream function (DSF), and the deformation power consumption was calculated. Aksakal et al. [16] studied the metal flow in the polygonal block forging process by the dual stream function and the upper bound method. The kinematically admissible velocity field of incompressible material was established.

The successful application of the stream function method in the forging and extrusion field makes many researchers study its application in the rolling process. Hwang et al. [17] analyzed the rolling process of the clad plate by the stream function method. Since then, Hwang et al. [18] established the mathematical model to calculate the velocity field for the plate rolling by using the double stream function method and cylindrical coordinates. The plastic deformation behavior of the sheet in the roll gap was studied. Sezek et al. [19] modified the inlet and outlet boundary conditions based on Hwang [17] and calculated the rolling power and rolling force. Ali [20] established a kinematically admissible velocity field model and supplied the upper bound solution of the model. Liu et al. [21] established the analytic model of the dog bone shape after rolling according to the DSF and the energy method. The stream function method plays an important role in the theoretic analysis of the rolling process which promotes the progress of the rolling industry and the rolling technology.

The main method to calculate the strain is the finite element method which requires an amount of memory and calculating time, and it is unsuitable to be used online with the millisecond level of calculating time. The slab method, upper bound method, energy method, and the stream function method have been used to analyze the rolling process except for the strain calculation. The purpose of this paper is to propose a theoretical model to calculate the equivalent strain online for the plate rolling with quick solution time. As a mature and reliable method, the stream function method and the energy method have been used to calculate the strain after rolling to avoid the complex stress analysis in this study. A kinematically admissible velocity field that is closed to reality and flexible enough to facilitate the calculation is established. The boundary conditions in the inlet and outlet of the roll gap are modified and optimized according to the characteristics of each deformation zone. The model error caused by the uniform deformation assumption is avoided by introducing the additional flow field with a parabolic line. A high precision linearized integral calculation method is adopted to ensure the calculation efficiency of the total consumption power. The equivalent strain after rolling is calculated on this basis. The rolling experiments and numerical simulation of AA1060 sheets are carried out to verify the validity and accuracy of the model. A reliable strain calculating model has been established in this paper and the obtained strain calculating model will provide reliable theory and technology support for the rolling production.

2. Theoretical parametric model

2.1 Geometric model

The following assumptions have been made to set up the equivalent strain calculation model after rolling.

1) The width expansion of the rolled plate with a large width to thickness ratio is so little after rolling. The three-dimensional plate rolling model can be simplified to be a two-dimensional planar strain model.

2) The elastic deformation and the elastic recovery after rolling are so little compared to the total deformation, so the rolled plate has been considered to be the ideal rigid-plastic material.

3) The deformation extent of the work rolls is smaller than the rolled piece, so the work rolls are considered as a rigid material.

4) The friction between the rolled piece and the work rolls conforms to Coulomb's friction law.

5) The deformation region of the rolled piece is divided into inlet rigid-plastic-outlet rigid zones according to the kinematics characteristics.

6) The velocity discontinuity is defined as the thin layer region (the thickness limit to zero) where the velocity changes rapidly and continuously at the boundary zone. The region is also the maximum shear stress position if the deformed body is in the plastic yield state. So the velocity discontinuity is used as the boundary between the rigid zone and the plastic zone in this paper.

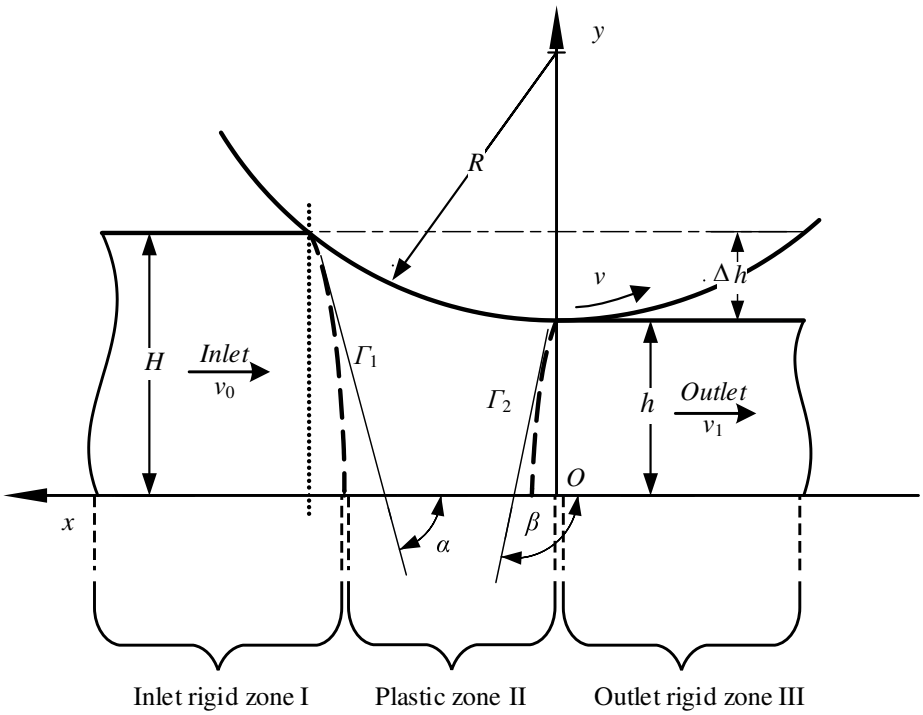

Fig. 1 Division of deformation region on the half thickness

The process parameters, geometric and the material model are symmetrical during the rolling process, so the half model can be selected for the strain calculating model establishment. As shown in **Figure 1**, the coordinate origin '*O*' locates at the central plate in the outlet cross section. The *x*-axis direction points to the opposite of the rolling direction. The *y*-axis direction points to the center of the top work roll.

2.2 Metal flow model

The deformation region is divided into three zones according to the deformation state and material flow characteristics. They are called the inlet rigid zone I, plastic deformation zone II,

outlet rigid zone III along the rolling direction as shown in Figure 1. The material flow path in the inlet rigid zone I and outlet rigid zone III are obtained according to the mass flow principle and material streamline in **Figure 2**.

In inlet rigid zone I

$$\Phi_{\mathrm{I}}=\varphi\frac{y}{H}=v_0 y\,. \quad (1)$$

In plastic zone II

$$\Phi_{\mathrm{II}}=\varphi\left\{\frac{y}{y_1(x)}+\left(ax^2+b\right)y\left[y-y_1(x)\right]\right\}, \quad (2)$$

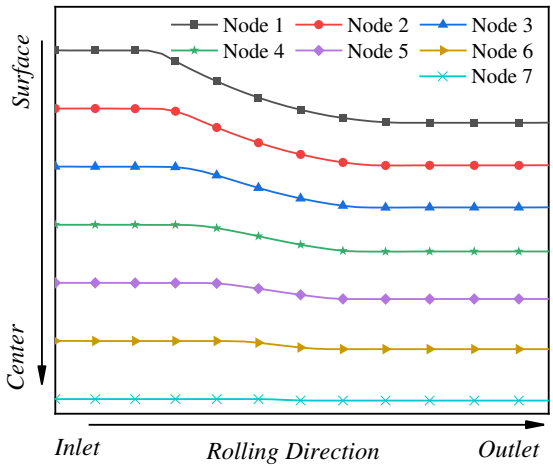

Fig. 2 Metal streamline

In outlet rigid zone III

$$\Phi_{\mathrm{III}}=\varphi\frac{y}{h}=v_1 y\,. \quad (3)$$

where φ is the mass flow in unit cross section, and $\varphi=V_0H=V_1h$. As shown in **Figure 2**, the streamline is closed to be parabolic in the plastic zone II. So the additional parabolic flow equation $y\ (ax^2 + b)\ [y\text{-}y_1(x)]$ is added to the uniform flow. The $y_1(x)$ is the geometric equation of rolling contact arc in plastic deformation zone II which can simplify as follows

$$y_1(x)=h+x^2/2R\,. \quad (4)$$

The deformation zones have the following relationship according to the continuous material the constant volume

$$\Phi_{\mathrm{I}}=\Phi_{\mathrm{II}}=\Phi_{\mathrm{III}}\text{ , (5)}$$

furthermore

$$\begin{aligned}\frac{y\varphi}{H}&=\varphi\left\{\frac{y}{y_1(x)}+\left(ax^2+b\right)y\left[y-y_1(x)\right]\right\}\\ \frac{y\varphi}{h}&=\varphi\left\{\frac{y}{y_1(x)}+\left(ax^2+b\right)y\left[y-y_1(x)\right]\right\}\end{aligned}\text{ . (6)}$$

The variable y is the only unknown variable in Equation 6 that expresses the coordinates in the plastic zone II.

The velocity discontinuities Γ_1 and Γ_2 are introduced as the boundary of the plastic zone II which can be expressed by Equation 6. Equation 7 can be obtained by shifting and eliminating the variable y based on Equation 6. Equation 7 represents the boundary condition of plastic deformation zone II. The velocity discontinuities can also be expressed as

$$\begin{cases}\Gamma_1: y_2(x)=\dfrac{1/H-1/y_1(x)}{ax^2+b}+y_1(x)\\ \Gamma_2: y_3(x)=\dfrac{1/h-1/y_1(x)}{ax^2+b}+y_1(x)\end{cases}\text{ . (7)}$$

The velocity components in plastic zone II can be derived from hydrodynamics theory. The velocity components are determined by the partial derivative function Φ_{II} to x and y

$$v_x=\frac{\partial\Phi_{\mathrm{II}}}{\partial y}=\varphi\left\{\frac{1}{y_1(x)}+\left(ax^2+b\right)\left[2y-y_1(x)\right]\right\}\text{, (8a)}$$

$$v_y=-\frac{\partial\Phi_{\mathrm{II}}}{\partial x}=\varphi y\left\{\frac{y_1'(x)}{y_1^{\,2}(x)}-2ax\left[y-y_1(x)\right]+\frac{x\left(ax^2+b\right)}{R}\right\}\text{. (8b)}$$

On this basis, the strain rate components in plastic zone II can be obtained by the partial derivative of Equation 8. Their expressions are as follows

$$\dot{\varepsilon}_x=\frac{\partial v_x}{\partial x}=\varphi\left\{-\frac{y_1'(x)}{y_1^{\,2}(x)}+2ax\left[2y-y_1(x)\right]-\left(ax^2+b\right)y_1'(x)\right\}\text{, (9a)}$$

$$\dot{\varepsilon}_y=\frac{\partial v_y}{\partial y}=\varphi\left\{\frac{y_1'(x)}{y_1^{\,2}(x)}-2ax\left[2y-y_1(x)\right]+\left(ax^2+b\right)y_1'(x)\right\}\text{. (9b)}$$

The sum of the strain rate component is zero according to the Equation 9 that is derived from the Equation 1-3, which is consistent with the constant volume criterion as shown in Equation

$$\dot{\varepsilon}_x + \dot{\varepsilon}_y = 0 \,. \quad (10)$$

2.3 Power model

The unknown variables *a* and *b* need to be confirmed by the optimal total power consumption model and then the mass flow in plastic zone II can be known. The tension is not existed for the plate rolling, so the tension can be ignored during the modeling process. The total power W_{all} in the half model is

$$W_{all} = W_V + W_\Gamma + W_f = W_V + W_{\Gamma_1} + W_{\Gamma_2} + W_f \,. \quad (11)$$

It is difficult to calculate the deformation power W_V due to the nonlinear Von-Mises yield criterion. The linearized yield criterion proposed by D.W. Zhao *et al.*[10] can facilitate the calculation of the deformation power W_V and ensure accuracy at the same time. And the integral operation along the *y* direction with the rotation coordinate system can significantly reduce the difficulty of the integral. The calculation model of plastic deformation power for the half rolling plate is as follows

$$\begin{aligned} W_V &= \frac{2\sqrt{3}}{3}\sigma_s[\int_0^h \int_{x_3(y)}^{x_2(y)} (\dot{\varepsilon}_{\max} - \dot{\varepsilon}_{\min}) dxdy + \int_h^H \int_{x_1(y)}^{x_2(y)} (\dot{\varepsilon}_{\max} - \dot{\varepsilon}_{\min}) dxdy] \\ &= \frac{4\sqrt{3}}{3}\sigma_s \left\{ \int_0^h \left[v_x \Big|_{x_3(y)}^{x_2(y)} \right] dy + \int_h^H \left[v_x \Big|_{x_1(y)}^{x_2(y)} \right] dy \right\} \end{aligned} \,, \quad (12)$$

where $x_2(y)$ and $x_3(y)$ are the inverse functions of geometric boundaries $y_2(x)$ and $y_3(x)$. It can be obtained from Equation (7). The expanded form of the integral term is

$$v_x\Big|_{x_3(y)}^{x_2(y)} = \frac{1}{H} - \frac{1}{h} + \left(2ay - ah - \frac{b}{2R}\right)\left[x_2^{\,2}(y) - x_3^{\,2}(y)\right] - \frac{a}{2R}\left[x_2^{\,2}(y) - x_3^{\,2}(y)\right]\left[x_2^{\,2}(y) + x_3^{\,2}(y)\right], \quad (13)$$

where $y_2(x)$ and $y_3(x)$ are inversely proportional to x^2 in Equation (8).

It is found that the Equation 12 is still a nonlinear integral equation after taking Equation 13 into Equation 12. The accuracy of the calculated results can be effectively guaranteed by using Gauss integral method with quintic accuracy.

The power consumed at the boundary of the deformation zone is called the velocity discontinuous power, and their expressed are as follows

$$\begin{cases} W_{\Gamma_1} = k\int_0^H \sqrt{\left(v_x - v_0\right)^2 + {v_y}^2}\, d\Gamma_1 \\ W_{\Gamma_2} = k\int_0^h \sqrt{\left(v_1 - v_x\right)^2 + {v_y}^2}\, d\Gamma_2 \end{cases}, \quad (13)$$

where the $d\Gamma_1$ and $d\Gamma_2$ are unit length on the velocity discontinuity lines, and it can be expressed as follows

$$\begin{cases} d\Gamma_1 = \sqrt{dx^2 + dy_2^2(x)} \\ d\Gamma_2 = \sqrt{dx^2 + dy_3^2(x)} \end{cases}. \quad (14)$$

Then Equation 13 becomes

$$\begin{cases} W_{\Gamma_1} = k\int_0^H \sqrt{\left(v_x - v_0\right)^2 + {v_y}^2} \cdot \sqrt{dx^2 + dy_2^2(x)} \\ W_{\Gamma_2} = k\int_0^h \sqrt{\left(v_1 - v_x\right)^2 + {v_y}^2} \cdot \sqrt{dx^2 + dy_3^2(x)} \end{cases}. \quad (15)$$

It is not difficult to find that the square root of the Equation 15 causes great difficulty in the solution. To solve this problem, the dx and $dy_2(x)$ (or $dy_3(x)$) which are in Equation 14 have the following relationship according to the geometric relation in **Figure 1**

$$\begin{cases} \tan\alpha = \dfrac{d\left[y_2(x)\right]}{dx} \\ \tan\beta = \dfrac{d\left[y_3(x)\right]}{dx} \end{cases}. \quad (16)$$

The $\tan\alpha$ and $\tan\beta$ presented in Equation 16 can be solved by the characteristics of the velocity discontinuity. Its expression is as follows

$$\vec{v}_0 \cdot \vec{n} = \vec{v} \cdot \vec{n}, \quad (17)$$

where $\vec{n}$ represents the normal vector at any node on Γ_1, Γ_2. So it can be known that

$$\begin{cases} -v_0 \sin\alpha = -v_x \sin\alpha + v_y \cos\alpha \\ v_1 \sin\beta = v_x \sin\beta + v_y \cos\beta \end{cases}, \quad (18)$$

and then

$$\begin{cases} \dfrac{v_y}{v_x - v_0} = \tan\alpha \\ \dfrac{v_y}{v_1 - v_x} = \tan\beta \end{cases}. \quad (19)$$

The angles between the tangent line and the x-axis for any point on Γ_1, Γ_2 are α and β respectively, and $\tan\alpha = d[y_2(x)]/dx$, $\tan\beta = d[y_3(x)]/dx$. So a relationship between the velocity and

the geometry will be built as follows

$$\begin{cases} \dfrac{v_y}{v_x - v_0} = \tan\alpha = \dfrac{d\left[y_2(x)\right]}{dx} \\ \dfrac{v_y}{v_1 - v_x} = \tan\beta = \dfrac{d\left[y_3(x)\right]}{dx} \end{cases} . \quad (20)$$

The simplified power consumption model during the deformation transition process is obtained by combining Equation 15 and Equation 20

$$\begin{cases} W_{\Gamma_1} = k\int_0^H \dfrac{\left(v_x - v_0\right)^2 + v_y{}^2}{v_y} dy \\ W_{\Gamma_2} = k\int_0^h \dfrac{\left(v_1 - v_x\right)^2 + v_y{}^2}{v_y} dy \end{cases} . \quad (21)$$

The friction power generated by the contact surface between the plate and the work rolls is as follows

$$\begin{aligned} W_f &= mk\int_0^{x_{n1}} \left(v_x - \omega R\cos\alpha\right) dx - mk\int_{x_{n1}}^{l} \left(v_x - \omega R\cos\alpha\right) dx \\ &= mk\omega R^2 \left[2\arctan\left(\frac{x_{n1}}{\sqrt{Rh}}\right)\left(1 + \frac{R}{h}\gamma^2\right)\sqrt{\frac{h}{R}} - \arctan\left(\frac{l}{\sqrt{Rh}}\right)\left(1 + \frac{R}{h}\gamma^2\right)\sqrt{\frac{h}{R}} + \left(\theta - 2\gamma\right) \right] . \quad (22) \end{aligned}$$

The total consumption power in the half thickness model can be obtained by adding deformation power, friction power and velocity discontinuities power. The *a* and *b* are calculated according to the principle of the minimum energy with the optimization theory and MATLAB optimization toolbox.

2.4 Equivalent strain model

The specific streamline in the plastic zone II can be calculated with the calculated *a* and *b* (in Equation 3). Then the kinematic parameters in the plastic zone II can be obtained by calculating the Equation 8 and Equation 9. The parameters obtained in Equation 9 are strain rates in plastic zone II. They cannot characterize the central equivalent strain after rolling. Therefore, it is necessary to calculate the generalized shear strain rate intensity to establish the equivalent strain calculation model.

$\dot{\Gamma}$ is the generalized shear strain rate intensity, and it can be expressed as

$$\dot{\Gamma} = 2\sqrt{\left|\dot{I}_2\right|} = 2\sqrt{\dot{\varepsilon}_x^2 + \dot{\varepsilon}_{xy}^2} . \quad (23)$$

On this basis, it is necessary to obtain the strain from the strain rate model. Λ is the cumulative value of the generalized shear strain rate intensity ($\dot{\Gamma}$), and its calculation model is

$$\Lambda=\int \dot{\Gamma}\, dt\,. \quad (24)$$

Finally, the equivalent strain model is expressed as follow

$$\varepsilon_e=\frac{\Lambda}{\sqrt{3}}\,. \quad (25)$$

The flowchart of the model is shown in **Figure 3**.

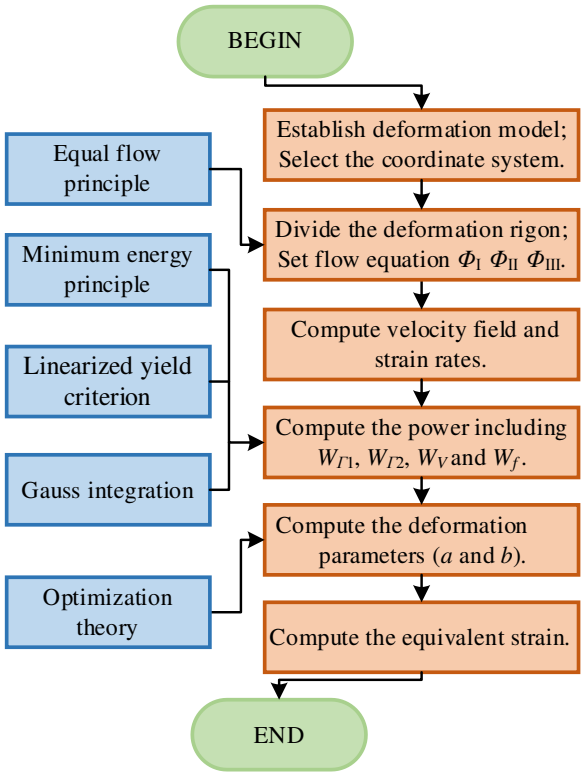

Fig. 3 Calculation flow chart

3. Results and discussion

3.1 Numerical modeling

Ansys/Ls-dyna software has been widely used in the deformation simulation, and the accuracy and reliability have been verified by many scholars according to the experiment. So the Ansys/Ls-dyna software was selected to use for the plate rolling process. The main parameters and speed parameters of the rolling were shown in Table 1 and the two-dimensional finite element model was shown in **Figure 4**.

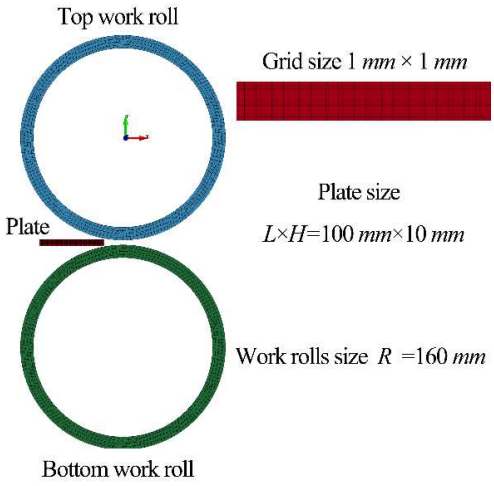

Fig. 4 The two-dimensional (2D) FEM model

Table 1 The main parameters used in FEM of plate

Item	Parameters	Value 1	Value 2
Work rolls	Radius [mm]	160	525
	velocity of the work rolls [m s^{-1}]	0.5	1.5
	Elastic modulus [GPa]	206	206
	Poisson ratio	0.25	0.25
Plate	Width [mm]	55	3000
	Length [mm]	100	2000
	Thickness [mm]	10	250
	Density [kg m^{-3}]	2705	7850
	Rolling reduction [mm]	2.5, 3, 3.5, 4, 4.5	50
	Yield stress [MPa]	39	100
	Elastic modulus [GPa]	62	110
	Tangent modulus [MPa]	105	10
	Poisson ratio	0.33	0.29
Other setting	Dynamic friction coefficient	0.2	0.35
	Static friction coefficient	0.25	0.40

As is shown in Figure 4, the geometric model includes the top work roll, bottom work roll, pinch rolls and the plate. The top and bottom work rolls are defined as rigid materials, and the rolled piece is defined as bilinear isotropic (BISO) material. The element type selected for the

simulation is 2D solid 162. The grid of rolled piece and the work rolls are 4 nodes elements (2D). The work rolls can only rotate about their axis. The rolled piece will be threatened into the roll gap by friction. The contact between the work rolls and the rolled piece is defined as 'contact-2D-automatic-single-surface'.

3.2 Experiment preparation

The plate rolling experiments were carried out in the laboratory by the rolling mill to ensure the reliability of numerical and analytical calculated results. The diameter of the work roll is 320mm which is the same as the 'value 1' in Table 1 and the other main process parameters were listed in Table 2. The tensile test was conducted for the aluminum alloy1060 plate and the stress-strain curves were obtained as shown in **Figure 5**.

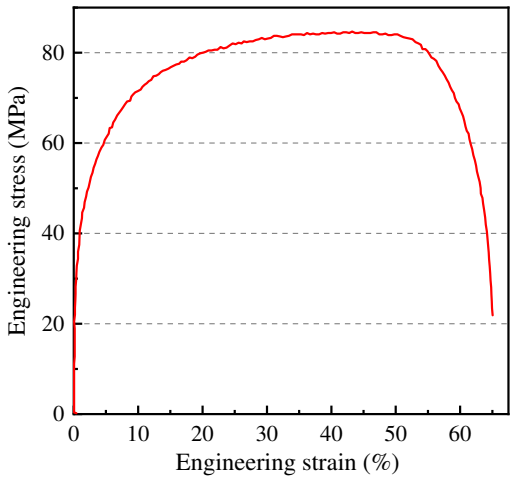

Fig. 5 Tensile stress-strain curves of the AA1060 plate

Table 2 The main parameters used in experiment

Geometric parameter	Plate 1	Plate 2	Plate 3	Plate 4	Plate 5
Initial thickness (mm)	9.75	9.85	9.87	9.85	9.87
Reduction (mm)	2.5	3	3.5	4	4.5
End thickness (mm)	7.12	6.61	6.17	5.78	5.4

The deformation characteristics of rolling materials were obtained by marking grids on the side. The grid was marking by laser along the thickness direction of rolled piece as shown in **Figure 6(a)**. The length and the height of the grid are 5mm and 1mm respectively on both sides, and the length and the height of the grid are all of 1 mm.

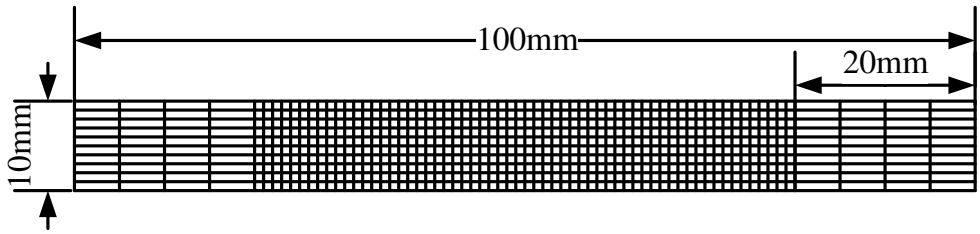

(a) The grid distribution before the experiment

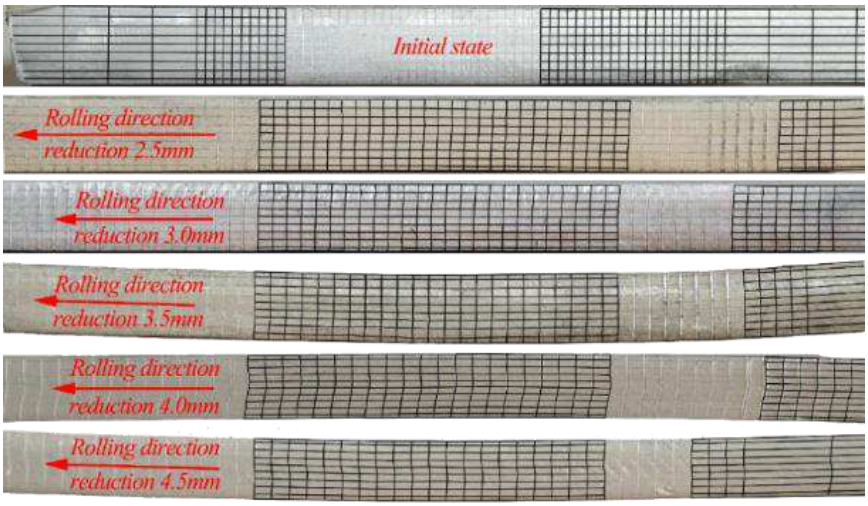

(b) The grid distribution after the experiments

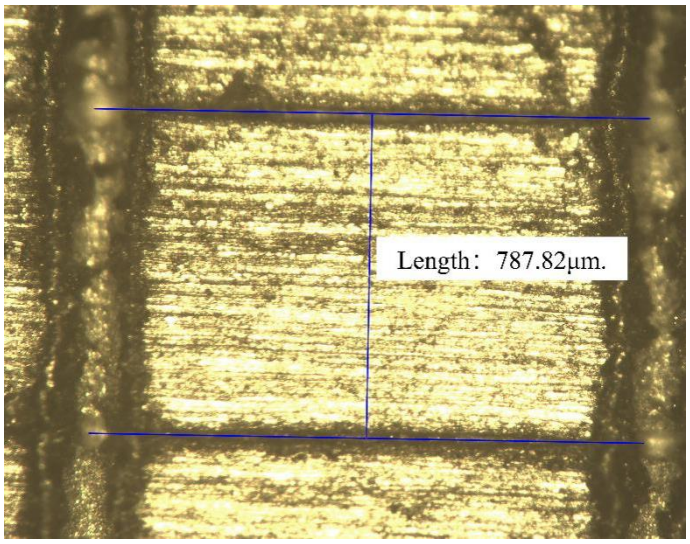

(c) The microgrid is measured by the microscope

Figure 6. Deformation of rolled piece

Figure 6 (b) shows the grid distribution after the experiment. The black deepened part in the middle of the picture is the stable rolling stage. The vertical grid line is changing with the increase of the rolling reduction. The actual micrograph is shown in **Figure 6 (c)**.

3.3 Calculated results and discussion

In order to verify the accuracy of the model established in this paper, the data in 3.1 Numerical simulation and 3.2 Experiment were extracted. The strain measured in the experiment is calculated as follows

$$\varepsilon = ln\ (h / h_0). \quad (24)$$

Figure 7 (a) shows the strain distribution in the center of the plate with a different calculated method. Figure 7 (b) shows the strain distribution at 1/4 thickness of the plate.

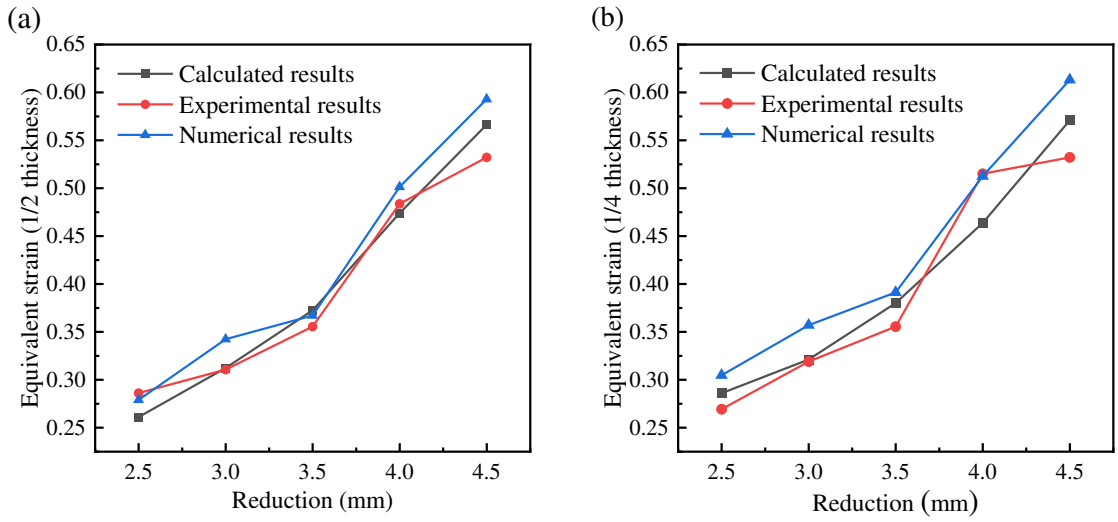

Fig. 7 Calculated results of equivalent strain in half and quarter thickness

The equivalent strain at the quarter thickness of the plate is higher than the center when the reduction is the same. This result validates the hypothesis of the non-uniform distribution of stress distribution in the calculation model. The accurate calculated results of each point in Figure 7 were shown in Table 3 and 4.

Table 3 The equivalent strain in half thickness

Rolling reduction	2.5 [mm]	3 [mm]	3.5 [mm]	4 [mm]	4.5 [mm]
Numerical results	0.2790	0.3423	0.3670	0.5013	0.5930
Experimental results	0.2861	0.3106	0.3555	0.4837	0.5321
Calculated results	0.2610	0.3122	0.3724	0.4739	0.5664
Relative error (N-E)	+2.54%	-9.26%	-3.13%	-3.51%	-10.27%
Relative error (N-C)	-6.45%	-8.79%	+1.47%	-5.47%	-4.49%
Relative error (E-C)	-8.77%	+0.52%	+4.75	-2.03%	6.45%

Table 4 The data of equivalent strain at 1/4 thickness

Rolling reduction	2.5 [mm]	3 [mm]	3.5 [mm]	4 [mm]	4.5 [mm]
Numerical results	0.3047	0.3570	0.3912	0.5125	0.6131
Experiment results	0.2692	0.3190	0.3614	0.5150	0.5486
Calculated results	0.2859	0.3211	0.3800	0.4637	0.5708
Relative error (N-E)	-11.65%	-10.64%	-7.61%	-0.49%	-10.52%
Relative error (N-C)	-1.88%	-10.06%	-2.86%	-9.52%	-6.90%
Relative error (E-C)	+6.20%	+0.66%	+5.15%	-9.96%	+4.04%

From the above analysis, the accuracy of the analytical model is high. In order to ensure the universality of the theoretical model, the material property is replaced by a hot-rolled carbon steel plate in the numerical results as shown in Table 1 (value 2). The accuracy of the model is verified by comparing the numerical results with the theoretical results. The strain distribution along the thickness direction is shown in **Figure 8**, and the numerical simulation and results are listed in Table 5.

Table 5 The main parameters used in FEM and theoretical calculation of thick plate

Y - Coordinates	5 [mm]	25 [mm]	45 [mm]	65 [mm]	85 [mm]	105 [mm]
Numerical results	0.130	0.145	0.186	0.276	0.367	0.386
Calculated results	0.1274	0.1625	0.1973	0.2838	0.3706	0.4167
Relative error	-2.0%	+12.07%	+6.08%	+2.83%	+0.98%	+7.95%

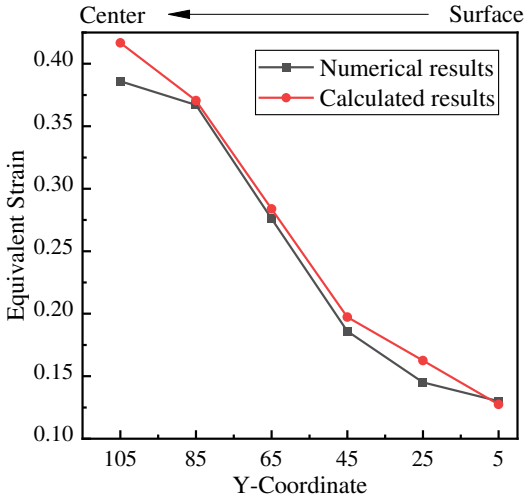

Fig. 8 Thickness direction strain results of thick plate

It can be seen that even if the material properties and geometric properties are changed, the accuracy of this model is still guaranteed. The maximum relative error of the strain is 12.07%, and the minimum relative error is 0.98% along the thickness direction.

4. Conclusion

This paper proposes a successful method to calculate the rolling strain after the plate rolling based on the stream function and the energy method. The main conclusions are as follows.

(1) The boundary conditions of adjacent deformation zones have been calculated and optimized according to the characteristics of each deformation zone, which makes the boundary condition close to the real situation. The kinematics partition method which makes the front slip zone and the back slip zone unified in the plastic zone II is adopted to avoid the complex stress analysis which will provide an important reference for the strain modeling.

(2) The rolling deformation region is divided into three zones (inlet rigid zone I, plastic zone II and outlet rigid zone III) according to the kinematics. The total power, the velocity field, and the shear strain rate were calculated and then the equivalent strain model was established on this basis by the minimum energy principle.

(3) The experiment and numerical simulation of the plate rolling were conducted to verify the strain model precision. The experimental and the numerical results showed that the minimum and maximum relative equivalent strain deviation between the analytic model and the experiment is 0.52% and 9.96% respectively. So the strain model established in this paper is reliable and accurate, which can be used for strain prediction online.

Availability of data and materials

Data and materials will be available upon request.

Author contributions

Lianyun Jiang: conceptualization; writing-original draft preparation; visualization; project administration

Yaoyu Wei: writing-original draft preparation; visualization

Heng Li: writing-review and editing; supervision

Lifeng Ma: writing-review and editing, supervision

Funding

The authors gratefully appreciate the financial support by the National Natural Science Foundation of China under Grant 51804206, the Major Science and Technology Projects in Shanxi under Grant 20181102016.

Declarations

Ethical approval Not applicable

Consent to participate Not applicable

Consent for publication Not applicable

Competing interests The authors declare no competing interests.

References

[1] Pan H, Cheng R, Du S, Xie H, Qin G (2020) Achieving high strength in micro-alloyed Mg-Al-Ca-Zn-Mn-Ce alloy sheet processed by single-pass large-strain rolling. J Mater Eng Perform 29(3): 1-10. https://doi.org/10.1007/s11665-020-05188-9.

[2] Zhang T, Wu YX, Gong H, Zheng XZ, Jiang SS (2014) Effects of rolling parameters of snake hot rolling on strain distribution of aluminum alloy 7075. T Nonferr Metal Soc 24(7): 2150-2156. https://doi.org/10.1016/S1003-6326(14)63326-4.

[3] Jiang LY, Zhao CJ, Shi JH, Yuan G, Wang XQ, Huang QX (2015) Hot rolled strip re-reddening temperature changing law during ultra-fast cooling. J Iron Steel Res Int 220(008): 694-702. https://doi.org/10.1016/S1006-706X(15)30059-5.

[4] A Hacquin, P Montmitonnet, J P Guillerault (1996) A steady state thermo-elastoviscoplastic finite element model of rolling with coupled thermo-elastic roll deformation. J Mater Process Technol 60(1): 109-116.https://doi.org/10.1016/0924-0136(96)02315-1.

[5] S H Hsiang, Lin SL(2001) Application of 3D FEM-slab method to shape rolling. Int J Mech Sci 43(5): 1155–1177. https://doi.org/10.1016/S0020-7403(00)00064-3.

[6] Denis Pustovoytov, Alexander Pesin, Olesya Biryukova (2018) Finite element analysis of strain gradients in aluminum alloy sheets processed by asymmetric rolling. Procedia Manufacturing 15: 129-136. https://doi.org/10.1016/j.promfg.2018.07.186.

[7] Bian S, Zhang XA, Li S, Zhang LA, Li W, Yan LB (2020) Numerical Simulation, Microstructure, properties of EH40 ultra-heavy plate under gradient temperature rolling. Mater Sci and Eng A: 791.

https://doi.org/10.1016/j.msea.2020.139778.

[8] Schmidtchen M, Kawalla R (2016) Fast numerical simulation of symmetric flat rolling processes for inhomogeneous materials using a layer model − part I: basic theory. Steel Res Int 87(8): 1065-1081. https://doi.org/10.1002/srin.201600047

[9] Jiang LY, Zhen T, Yuan G, Huang JB, Wei YY, Li H, Wang P (2020) The mechanical parameters modeling of heavy steel plate snake/gradient temperature rolling with the same roll diameters. Metall Res Technol 117(3): 301. https://doi.org/10.1051/metal/2020019.

[10] Zhao DW, Zhang SH, Li CM, Song HY, Wang GD (2012) Rolling with simplified stream function velocity and strain rate vector inner product. J Iron Steel Res Int 19(003): 20-24. https://doi.org/10.1016/S1006-706X(12)60068-5.

[11] Zhang SH, Song BN, Gao SW, Guan M, Zhou J, Chen XD, Zhao DW (2018) Upper bound analysis of a shape-dependent criterion for closing central rectangular defects during hot rolling. Appl Math Model 55(MAR.): 674-684. https://doi.org/10.1016/j.apm.2017.11.012.

[12] SI Oh, Shiro Kobayashi (1975) An approximate method for a three-dimensional analysis of rolling. Int J of Mech Sci 17(4) :293-305. https://doi.org/10.1016/0020-7403(75)90010-7.

[13] Laila S Bayoumi (1998) Flow and stresses in round–oval–round roll pass sequence. Int J Mech Sci 40(12): 1223-1234.https: //doi.org/10.1016/S0020-7403(98)00005-8.

[14] Wang JP, Lin YT (1995) The load analysis of the plane-strain forging processes using the upper-bound stream-function elemental technique. J Mater Process Tech 47(3-4): 345-359. https://doi.org/10.1016/0924-0136(95)85008-2.

[15] KP Maity, P K Kar, NS Das (1996) A class of upper-bound solutions for the extrusion of square shapes from square billets through curved dies. J Mater Process Tech 62(1-3): 185-190. https://doi.org/10.1016/0924-0136(95)02228-7.

[16] B Aksakal, S Sezek, Y Can (2005) Forging of polygonal discs using the dual stream functions. Mater Design 26(8): 643-654. https://doi.org/10.1016/j.matdes.2004.09.005.

[17] YM Hwang, HH Hsu, HJ Lee (1995) Analysis of sandwich sheet rolling by stream function method. Int J Mech Sci 39(3):598-605. https://doi.org/10.1016/0020-7403(95)93522-8.

[18]YM Hwang, HH Hsu (1998) Analysis of plate rolling using the dual-stream function method and cylindrical coordinates. Int J Mech Sci 40(4): 371-385. https://doi.org/10.1016/S0020-7403(97)00040-4.

[19] S Sezek, B Aksakal, Y Can (2008) Analysis of cold and hot plate rolling using dual stream functions.

Mater Design 29(3): 584-596. https://doi.org/10.1016/j.matdes.2007.03.005.

[20] Ali Nuri Doğruoğlu (2001) On constructing kinematically admissible velocity fields in cold sheet rolling. J Mater Process Tech 110(3): 287-299. https://doi.org/10.1016/S0924-0136(00)00897-9.

[21] Liu YM, Zhang DH, Zhao DW, Sun J (2016) Analysis of vertical rolling using double parabolic model and stream function velocity field. Int J Adv Manuf Technol 82(5-8): 1153–1161. https://doi.org/10.1007/s00170-015-7393-7